Sylvie Le Hégarat-Mascle
Isabelle Bloch
Emanuel Aldea (Eds.)

LNAI 13506

Belief Functions: Theory and Applications

7th International Conference, BELIEF 2022
Paris, France, October 26–28, 2022
Proceedings

Springer

Evidential Filtering and Spatio-Temporal Gradient for Micro-movements Analysis in the Context of Bedsores Prevention

Nicolas Sutton-Charani[1(✉)], Francis Faux[2], Didier Delignières[1], Willy Fagard[3], Arnaud Dupeyron[3], and Marie Nourrisson[2]

[1] EuroMov Digital Health in Motion, Univ Montpellier, IMT Mines Ales, 6 Avenue de Claviéres, 30100 Alés, France
nicolas.sutton-charani@mines-ales.fr, didier.delignieres@umontpellier.fr

[2] ISIS Engineer School, Castres, France
francis.faux@irit.fr, marie.nourrisson@etud.univ-jfc.fr

[3] CHU de Nîmes, Nîmes, France
willy.fagard@chu.nimes.fr, arnaud.dupeyron@umontpellier.fr

Abstract. In the context of pressure ulcer prevention, this article deals with the problem of detecting and analysing micro-movements in the sacral area of bedridden patients on mattresses equipped with a network of pressure sensors. The study is based on a series of pressure measurements carried out on a cohort of patients lying on two types of mattress at the Nîmes university hospital (France). A spatio-temporal model considers first the local information of measurements from the array of sensors using an evidential filter in order to remove spatial uncertainties or measurement noise before micro-movement analysis. With a Detrended Fluctuation Analysis (DFA), the complexity level of the time series coming from the micro-movement model is finally estimated for different noise filters.

Keywords: Bedsores prevention · Micromovements analysis · Spatio-temporal gradient · Pressure sensors · Detrended fluctuation analysis

1 Introduction

Pressure ulcers, also known as 'bedsores', refer to a type of injury that necroses the skin and underlying tissue because of large amount of pressure applied to an area of skin over a short period. Due to their lack of muscle, elderly people and individuals with severely compromised states of health are especially vulnerable to pressure sores [1]. Prevention of pressure ulcer formation is primarily focused on minimizing episodes of prolonged pressure either by placing appropriate padding at pressure points or by frequent patient repositioning [10,12].

In 2015, the laboratory of Bio-Statistics, Clinical Epidemiology, Public Health, Innovation and Methodology (BCPIM) attached to the Nîmes hospital (France) carried out a series of measurements using a connected pressure

S. Le Hégarat-Mascle et al. (Eds.): BELIEF 2022, LNAI 13506, pp. 297–306, 2022.
https://doi.org/10.1007/978-3-031-17801-6_28

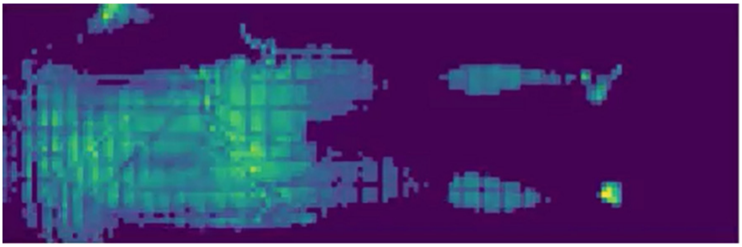

Fig. 1. Pressure image (patient 5, mattress Softform)

48 × 145 uniform sensor array sited on top of mattresses, over a period of 1 month, in order to evaluate the levels of pressure exerted by the mattress on bed ridden patients. The pressure measurements lie in [0 mmHg, 100 mmHg] with a precision of 0.1 mmHg. This study based on the statistical analysis of pressure peaks has highlighted high variability and non-reproducibility between measurements [13]. The measures have been carried out on a cohort of patients spread over 3 centers located in Occitanie (France): CHU Nîmes, EHPAD9 La Chimotaie, EHPAD Notre Dame des Pins. Each center realised measurements on patients lying on two different mattress models: Softform or Airsoft. For each measurement of 30 min, the software recorded the pressure values coming from the sensor network at a frequency of one per second. Hence, we can observe the profile of the patient lying on the bed every second (see Fig. 1). In this paper we pursue this study by considering, instead of the pressure peaks, the spatio-temporal distribution of pressure variations assumed to be caused by micro-movements in the sacral region. These micro-movements are supposed to result from many different processes such as blood pressure, muscular and neural impulsions, or mobility of the tissues when the patients remain immobile in hospital beds. It turns out that the specificity of micro-movements is difficult to observe. According to Descartes a movement refers to the action by which a body moves from one place to another [3]. The concept of *movement* thus generally implies some shape preservation. In our context, the shape in movement is poorly known, not rigid and deformable. Hence, classical image motion analysis methods (optical flow) appears not applicable. Another difficulty raises in the differentiation between micro-movements and disturbing noise due to sensors uncertainties (imprecision, reliability). In the domain of image processing, many approaches have been proposed to search for efficient image denoising [2]. In the framework of Dempster-Shafer theory, this problem has been discussed by Weeraddan et al. in [16] in order to process temporally and spatially distributed multi modality sensor data. The authors extended Temporal Evidence Filtering [6], that allows to merge multi-modalities evidence and to infer in the frequency domain but they do not address the problem of noise buried in the information clutter. In a study close to our problematic, carried out by Li et al. [11] in the domain of visual tracking, the authors incorporate Dempster-Shafer information fusion into the entire image sequence partitioned into spatially and temporally

adjacent sub-sequences. However these models do not respond to our specific context of sparse data, i.e., grey scale images containing many null values. The model of micro-movements proposed in this paper integrates the uncertainty in motion detection using a spatio-temporal gradient method and an evidential filter necessary to smooth, in an adequate way, pictures of pressure levels. Finally a Detrended Fluctuation Analysis (DFA) is proposed to compare in term of complexity the proposed micro-movements model in regards to classic filtering techniques.

The organisation of the rest paper is as follows. In Sect. 2 we recall the necessary basis of the belief function theory and we briefly recall the Detrended Fluctuation Analysis (DFA) for time series complexity estimation. Section 3 presents the evidential filter based on the EKNN model [5] and the micro-movements quantification method. Experiments and results are detailed in Sect. 4 and finally we present our concluding remarks and perspectives.

2 Necessary Background

2.1 Belief Function Theory

In Belief function theory [14], uncertainty regarding the value of a variable ω defined on a finite set of possible values, called the frame of discernment $\Omega = \{\omega_1, \ldots, \omega_N\}$ is represented by a basic belief assignment (BBA) or mass function m defined as a mapping $m : 2^\Omega \rightarrow [0, 1]$ verifying $\sum\limits_{A \subseteq \Omega} m(A) = 1$.

The conjunctive combination of BBA's m_j derived from J distinct sources, denoted by $m_{\bigcap}$ is expressed by $m_{\bigcap}(A) = \sum_{A_1 \cap \ldots \cap A_J = A} \left(\prod_{j=1}^{J} m_j(A_j)\right)$. Dempster's rule, denoted by $\oplus$, is a normalized version of the conjunctive combination rule and is defined such that: $m_\oplus(\emptyset) = 0$ and $m_\oplus(A) = K \cdot m_{\bigcap}$ for $A \neq \emptyset$. The normalization factor K is of the form $(1 - c(m_1, \ldots m_J))^{-1}$ where $c(m_1, \ldots m_J) = \sum\limits_{A_1 \cap \ldots \cap A_J = \emptyset} \left(\prod_{j=1}^{J} m_j(A_j)\right)$ represents the amount of conflict between the sources. These two combination rules are commutative, associative, and often used to combine BBAs from distinct sources.

The pignistic transformation [15] distributes the ignorance equally among each singleton element in Ω such that:

$$BetP(\omega) = \frac{1}{\Big(1 - m(\emptyset)\Big)} \sum_{W \subseteq \Omega : W \ni \omega} \frac{m(W)}{|W|}$$

where $|W|$ is the number of singletons in W, we have $\sum\limits_{\omega \in \Omega} BetP(\omega) = 1$.

2.2 Detrended Fluctuation Analysis (DFA)

The complexity of biological signals has given rise to many research works [4,7, 17]. Among several alternatives (e.g. entropy), Detrended Fluctuation Analysis

(DFA) provides fractality level estimators of any signal, even non-stationary ones, and has shown to efficiently discriminate healthy and ill subjects [8,9].

The DFA algorithm works as follow, for a series $x(i)$ of length N. The series is first integrated, by computing for each i the accumulated departure from the mean of the whole series: $X(i) = \sum_{j=1}^{i} \left(x(j) - \bar{x}\right)$ where $\bar{x} = \sum_{i=1}^{N} x(i)$.

This integrated series is then divided into k non-overlapping intervals of length n. The last $N - kn$ data points are excluded from analysis. Within each interval, a least squares line is fitted to the data. The series $X(i)$ is then locally detrended by subtracting the theoretical values $X^{Th}(i)$ given by the regression. For a given interval of length n, the characteristic size of fluctuation for this integrated and detrended series is calculated by:

$$F(n) = \sqrt{\frac{1}{N - kn} \sum_{i=1}^{N-kn} \left(X(i) - X^{Th}(i)\right)^2}.$$

This computation is repeated over a large range of interval lengths. In the present experiment, from $n = 10$ to $n = 300$, by steps of 1. A power law is expected between n and the average fluctuation size $F(n)$, as $F(n) \propto n^{\alpha}$.

The exponent α is estimated as the slope of the double logarithmic plot of $F(n)$, as a linear function of n. Typically, $\alpha = 1$ corresponds to an optimal complexity level, generally encountered in healthy, and perennial systems. $\alpha = 0.5$ reveals uncorrelated white noise series, and denotes a complete loss of complexity in the underlying system. At the opposite, $\alpha \approx 1.5$ for quasi-deterministic systems having almost no adaptability.

3 Method

In this section we present an evidential extension of the median (or mean) filter, we propose a micro-movement measure and we explain how the filtering method can impact the micro-movement complexity signal.

3.1 Evidential Filter

The median filter is one of the most famous approach to remove noise from images. It is a non-linear filter which has the property of preserving edges while removing noise. However it is not appropriate for sparse data, e.g. grey scale images containing many null values. Indeed, in that context, the mean filter seems to give better results (see Fig. 2) probably due to higher number of possible estimate, especially for data with frequent values (0 or 1 often arise with pressure sensors). In the bedsores problem, a grid pattern which comes from structural sensors array defect, is visible on all pressure images. This type of perturbation makes necessary some filtering upstream of any analysis.

The idea of our proposal is to use the local information of the sensors array in order to denoise the images before micro-movement analysis and to asses to filter's choice impact in terms of micro-movements and associated complexity. The belief function framework is used in order to take advantage of its uncertainty modelling and fusion abilities. Our model is based on the spatial uncertainty model proposed by Denœux in [5] which extends the K-NN algorithm to uncertain labels where neighbours are considered as information sources with a reliability level that depends on their similarity to the prediction example. The corresponding spatial uncertainty model is recalled hereafter:

$$\begin{cases} m^{s,i}(C_q) = \alpha \\ m^{s,i}(C) \ = 1 - \alpha \end{cases} \quad \text{with} \quad \alpha = \alpha_0 e^{-\gamma_q d^\beta} \tag{1}$$

where $m^{s,i}$ is the mass function representing the reliability of neighbour x_i, in regards to a new example x_s to classify, y_i is the label of x_i, which is supposed to belong to class C_q, C is the set of all possible classes and d stands for the distance between x_s and x_i. The $(\alpha_0, \gamma_q, \beta)$ coefficients are tuning hyper-parameters.

With pressure images, as for median and mean filters we slide windows and replace the center of the window by a certain value which is neither the median nor the mean value of the window but is computed as the pignistic expectation of the conjunctive fusion of the window sensors. For a given pixel window, for all pressure measurements a mass function is defined according to the $EKNN$ spatial uncertainty model (1) extended to the numerical context by replacing the categorical focal elements C_q by numerical ones ω_i which stands for the pressure measurement of a pixel i. In our approach we chose to redefine the frame of discernment $\Omega = \{w_1, ..., w_K\} \subseteq \{p_1, ..., p_N\} \subset R^+$ for each window of N pixels as the set of K different observed pressure values. By definition, $\forall_i \neq j : w_i \neq w_j$ but the observed pressures can be identical for several pixels of a window, we have $K \leq N$.

The adaptation of the $EKNN$ spatial uncertainty model to the pressure sensors context is given in Eq. (2).

$\forall_i = 1, \cdots, N$:

$$\begin{cases} m_i\left(p_i\right) = \alpha_i \\ m_i\left(\Omega\right) = 1 - \alpha_i \end{cases} \tag{2}$$

with $\alpha_i = \alpha_0 e^{-\gamma d_i^\beta}$. The distance d_i is computed between the i^{th} pixel having for pressure value p_i and the center of the window.

The conjonctive combination of all the window pixels mass functions leads to a final mass function m^* having for focal elements all the window pixel single values and Ω.

$$\begin{cases} \forall k = 1, ..., K : \\ m^*\Big(\{w_k\}\Big) = \dfrac{\prod\limits_{\substack{i=1 \\ p_i = w_k}}^{N} \alpha_i \times \prod\limits_{\substack{j=1 \\ p_j \neq w_k}}^{N} (1-\alpha_j)}{1-\kappa} \\ m^*\Big(\{w_1, ..., w_K\}\Big) = \dfrac{\prod\limits_{i=1}^{N} (1-\alpha_i)}{1-\kappa} \end{cases} \tag{3}$$

with

$$\kappa = 1 - \sum_{k=1}^{K} \Big[\prod_{\substack{i=1 \\ p_i = w_k}}^{N} \alpha_i \times \prod_{\substack{j=1 \\ p_j \neq w_k}}^{N} (1 - \alpha_j) + \prod_{i=1}^{N} (1 - \alpha_i) \Big]$$

As a first approach we propose to compute the pignistic transform $BetP^*$ of m^* and to replace the central pixel s of the window by the expectation of an unknown pressure value W according to the $BetP^*$ probability.

Results of the pignistic transform applied to m^* and the corresponding expectation of an uncertain pressure value W are given in Eqs. (4) and (5).

$\forall k = 1, ..., K$,

$$BetP^*\Big(\{W = w_k\}\Big) = m^*\Big(\{w_k\}\Big) + \frac{1}{K} m^*\Big(\Omega\Big) \tag{4}$$

$$E_{BetP^*}\Big[W\Big] = \sum_{k=1}^{K} w_k * BetP^*\Big(\{W = w_k\}\Big) \tag{5}$$

The choice of redefining the frame of discernment Ω for each pixels window comes from the local nature of the belief filter, we only take into account the of pixels neighbors to smooth images. The fact that we consider discrete spaces Ω is counterbalanced by the pignistic transform which can result in any value between the elements of Ω (see Eq. (5)).

The belief filter we propose smooth the pressure images with a sliding window approach. For all pixel windows the central pixel is replaced by the pignistic expectation of the (uncertain) pressure values of all its neighbors and their corresponding bbas which are defined according their distance to the central pixel (see Eq. (3)). In the following subsection we propose a micro-movement indicator which can be computed on any sets of pressure images, smoothed or not.

3.2 Micro-movements Quantification

Once all images have been smoothed with our belief filter, we quantify the amount of micro-movement as the level of deformation enhanced by variations of pressure on the sensor network. Indeed, all the information available about these movements is provided by pressure sensors which provide grey intensity images at each timestamp.

A sequence of pressure measurements images can be considered as a 3-dimensional discrete spatio-temporal field: $W_t^{(x,y)}$, where x and y denote the coordinates of an individual sensor in the sensor network, and t is the time index. The gradient vector $\vec{\nabla}(W_t^{(x,y)})$ is defined such that $\vec{\nabla} = [\partial/(\partial x), (\partial/\partial y)]^T$. The Sobel operator allows to calculate approximations of the horizontal and vertical derivatives using two 3×3 kernels which are convolved with the original source image $W_t^{(x,y)}$. The Sobel operator allows to calculate two images

$S_x(t) = \begin{pmatrix} 1 & 0 & -1 \\ 2 & 0 & -2 \\ 1 & 0 & -1 \end{pmatrix} \star W_t^{(x,y)}$ and $S_y(t) = \begin{pmatrix} 1 & 2 & 1 \\ 0 & 0 & 0 \\ -1 & -2 & -1 \end{pmatrix} \star W_t^{(x,y)}$ which contain respectively the horizontal and vertical approximations of the gradient vector for each point (x, y). The 2-dimensional signal processing convolution operation is denoted by $\star$.

The micro-movement measure μ_{mvt} is computed as the absolute value of the spatio-temporal gradient of the videos corresponding to the set of pressure images of one measurement of 30 min:

$$\mu_{mvt}(t, x, y) = \left| \frac{\partial}{\partial t} S(t, x, y) \right| \tag{6}$$

where $S(t, x, y) = \sqrt{S_x(t)^2 + S_y(t)^2}$.

It is noticeable that micro-movements quantification can be computed independently of the considered filter, even on raw image (without any filtering). In the case of filtered images, the Sobel values $S(t, x, y)$ are computed on images that have been smothed according to Eqs. (3) and (5).

4 Experiment and Results

In this section the evaluation criteria considered in this study are detailed and finally results are presented in terms of filtering, micro-movement and DFA.

The evidential filtering proposed in this work is first visually evaluated. The micro-movement and complexity time series computed on raw and filtered images are compared. This comparison is realised with the raw signals as reference, *i.e.,* the best denoising filters corresponding to the closest micro-movement and complexity signals to the ones computed on raw images (without filtering).

Visual Evaluation of Filtering (Fig. 2). The median filtered images are very smoothed which is not an optimal context for micro-movement analysis since micro-movements are of very low intensity by definition. The belief filter gives a less smoothed image than the mean filter (the grid has almost disappeared), which is suitable for the analysis of of micro-movements that could become undetectable with too strong smoothing.

Micro-movement Quantification

The micro-movement signal computed as in Eq. (6) contains large peaks which do not correspond to micro-movement but are rather due to real movements when the patient lies down on his bed. In order to extract those real movements from the signal, we removed upstream all micro-movement data that were higher than the 99^{th} signal centile. The obtained micro-movement time series seems stationary and rough enough for complexity computations.

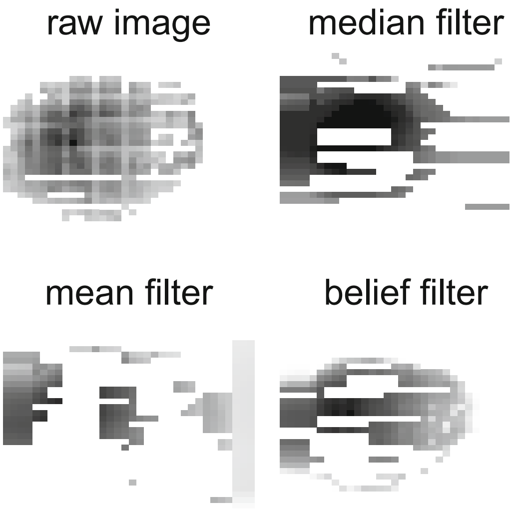

Fig. 2. Sacrum denoising

In terms of DFA

For three measurements, the evolution of complexity is presented in Fig. 3, nevertheless all the following comments have been made on the set of 18 measurements.

We first observe that for all three filters (median, mean and belief) the same curve shapes are observed. This means that the filter choice has no impact on the complexity evolution shape. However, the filtered level of complexity computations are generally biased from the ones computed on raw images and these biases tend to decrease with time. On the set of 18 measurements we note that the raw complexity signals lie almost always between filtered signals, except for 2 or 3 cases when the raw complexity signal has especially large variations probably due to some real movement track perturbations. In terms of DFA, this seems to attenuate the filter choice importance and even the importance of filtering itself which is sometimes a delicate pre-processing question for analysts and researchers.

Finally, in terms of filtering, mean and belief filters curves are always very close. However, significance test comparison have been made on the final levels of complexity in order to compare the complexity estimation absolute errors (in regards to the final complexity level computed on raw images). On the set of 18 measurement the median filters complexity estimator has the lowest error: 0.0154, the belief and mean filter having errors of 0.0161 and 0.0380. With a risk of 5% there is no significant (Wilcoxon test) difference of complexity estimation errors between median and belief filters ($p = 0.290$) whereas belief filter estimation errors are significantly lower than mean filter one ($p = 0.009$).

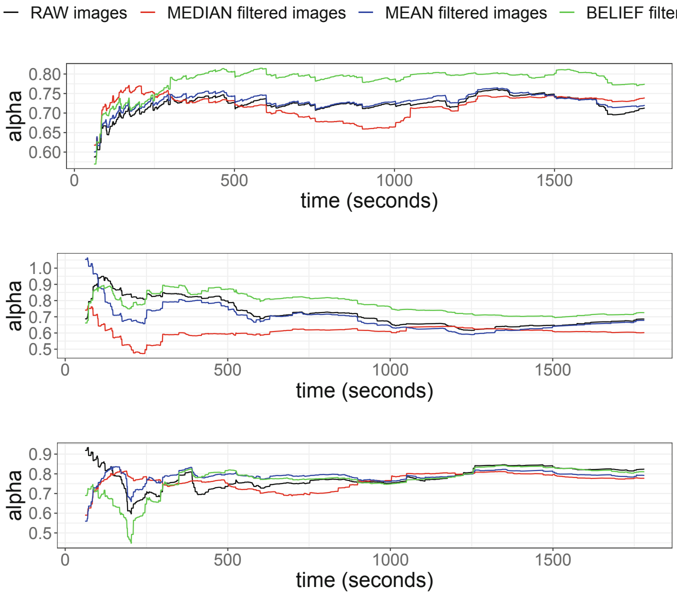

Fig. 3. Filtering vs complexity

5 Conclusion and Perspectives

In this paper a spatio-temporal model of micro-movement located in the sacral area of bedridden patients has been proposed as weel as a study of the evolution of complexity during the measurement (30 min). This preliminary work lays the foundations for a micro-movement analysis integrating uncertainty/imprecision management using an evidential filter. Results are encouraging.

In standard DFA, the complexity parameter α is computed on the whole signal, *i.e.* once the measurement is complete. In our case we monitored the evolution of complexity over time in order to estimate the necessary measurement duration to get a relatively stable level of sacrum micro-movement complexity (α coefficient). Concerning DFA, the measurement noise does not seem to impact the estimates and it does not seem necessary to filter for complexity analysis.

In an industrial perspective this type of estimation could be of precious value for connected mattresses and bedsores risk notifications (when the amount of micro-movement is too low or the level of complexity seems abnormal).

The future works concern the search of a similarity measure able to discriminate patients and mattresses from micro-movement and complexity signals based on machine learning methods. In the evidential perspective, uncertainty modeling should be improved with more complex fusion and decision rules and finally it would be interesting to consider uncertainties at the complexity level in the DFA model.

References

1. Bhattacharya, S., Mishra, R.: Pressure ulcers: current understanding and newer modalities of treatment. Indian J. Plast. Surg. **48**(01), 004–016 (2015)
2. Buades, A., Coll, B., Morel, J.M.: A review of image denoising algorithms, with a new one. Multisc. Model. Simul. **4**(2), 490–530 (2005)
3. Clavelin, M.: Galilée et Descartes sur la conservation du mouvement acquis, vol. 242[1]. Dix-septiéme siécle (2009)
4. Delignieres, D., Lemoine, L., Ramdani, S., Torre, K., Fortes, M., Ninot, G.: Fractal analyses for "short" time series: a re-assessment of classical methods. J. Math. Psychol. **50**, 525–544 (2000)
5. Denæux, T.: A k-nearest neighbor classification rule based on Dempster-Shafer theory. IEEE Trans. Syst. Man Cybern. **219**, 804–813 (1995)
6. Dewasurendra, D.A., Bauer, P.H., Premaratne, K.: Evidence filtering. IEEE Trans. Signal Process. **55**(12), 5796–5805 (2007)
7. Eke, A., Herman, P., Kocsis, L., Kozak, L.: Fractal characterization of complexity in physiological temporal signals. Physiol. Meas. **23**, 31–38 (2002)
8. Goldberger, A.L., Amaral, L.A.N., Hausdorff, J.M., Ivanov, P.C., Peng, C.K., Stanle, H.E.: Fractal dynamics in physiology: alterations with disease and aging. Proc. Natl. Acad. Sci. **99**(suppl_1), 2466–2472 (2002)
9. Hausdorff, J., et al.: Altered fractal dynamics of gait: reduced stride-interval correlations with aging and Huntington's disease. J. Appl. Physiol. (Bethesda, Md. : 1985) **82**, 262–9 (1997)
10. Kim, S.Y., Shin, Y.S.: A comparative study of 2-hour interface pressure in different angles of laterally inclined, supine, and fowler's position. Int. J. Environ. Res. Public Health **18**(19), 9992 (2021)
11. Li, X., Dick, A., Shen, C., Zhang, Z., van den Hengel, A., Wang, H.: Visual tracking with spatio-temporal Dempster-Shafer information fusion. IEEE Trans. Image Process. **22**(8), 3028–3040 (2013)
12. Mervis, J.S., Phillips, T.J.: Pressure ulcers: Prevention and management. J. Am. Acad. Dermatol. **81**(4), 893–902 (2019)
13. Neverov, C., et al.: Modélisation incertaine à partir de mesures non-reproductibles. Application à la comparaison de pression exercée par des matelas. In: LFA 2019–28ème Rencontres Francophones sur la Logique Floue et ses Applications. Alès, France (2019)
14. Shafer, G.: A mathematical theory of evidence. In: A Mathematical Theory of Evidence. Princeton University Press (1976)
15. Smets, P.: Decision making in the TBM: the necessity of the pignistic transformation. Int. J. Approx. Reason. **38**(2), 133–147 (2005)
16. Weeraddana, D.M., Kulasekere, C., Walgama, K.S.: Dempster-Shafer information filtering framework: temporal and spatio-temporal evidence filtering. IEEE Sens. J. **15**(10), 5576–5583 (2015)
17. West, B.J.: Fractal Physiology and Chaos in Medicine, 2nd edn. World Scientific, Singapore (1990). https://doi.org/10.1142/8577